2024 IEEE/RSJ International Conference on Intelligent Robots and Systems (IROS)
October 14-18, 2024. Abu Dhabi, UAE

An Agile Robotic Penguin Driven by Submersible Geared Servomotors: Various Maneuvers by Active Feathering of the Wings

Taiki Shimooka, Atsushi Kakogawa, and Hiroto Tanaka

Abstract—**This study introduces an agile robotic penguin featuring a pair of 2-degrees of freedom (DoF) wing mechanisms. Each wing can independently control flapping and feathering motions with two in-house submersible geared servomotors through a differential gear mechanism. Notably, our mechanism allows unrestricted feathering beyond 360°. Since feathering directly changes the wing's angle of attack (AoA), the hydrodynamic forces can be significantly adjusted to achieve agile maneuvers. This paper demonstrates various maneuvers, including rapid acceleration, hard braking, rolling, pitching, and yawing, achieved solely by changing the feathering motion of both wings. Our robotic penguin reached a maximum forward speed of 1.8 m/s, comparable to the foraging speed of real penguins. The average roll, pitch, and yaw rates were 363°/s, 75°/s, and 92°/s, respectively. This robot serves as a model for the biological study of maneuverability in real penguins and the engineering exploration of bioinspired agile underwater robots.**

I. Introduction

Swimming animals are promising models for the development of future underwater remotely operated vehicles (ROVs) and autonomous underwater vehicles (AUVs) that are agile, efficient, and fast in complex and unsteady conditions, such as wild environments [1]. Research has led to the development of various biomimetic robots inspired by marine life, such as fish [2 – 5], dolphins [6], rays [7], jellyfish [8], and even bivalves [9]. Their propulsion methods can generally be classified into oscillation or wave-like undulation of a tail wing or body, oscillation or wave-like undulation of a pair of lateral wings or fins, and water jetting [10, 11]. Among these, the oscillation of lateral wings provides superior agility, while the high-frequency oscillation of a tail fin enables high-speed propulsion [12].

Penguins are diving birds that propel themselves by a pair of flapping wings, exhibiting excellent swimming abilities, such as sustained high-speed foraging at more than 2.0 m/s [13], long distance of travel exceeding 200 km per day [14], and high turning rates of up to 576°/s [15]. The key feature of their maneuverability is their ability to feather their wings which involves rotating the wing around its long axis to alter the angle of attack (AoA) relative to incoming flow. This rotation directly changes the magnitude and direction of the generated thrust. A few studies have attempted to replicate this penguin-like flapping-wing swimming in underwater robots. The AquaPenguin developed by Festo AG. & Co. KG, achieved controlled free diving without a tether [16]. In this design, the feathering of the left and right wings was independently controlled by separate motors. However, the wings were mechanically connected, and flapping was driven by a single motor, resulting in limitations in wing motion. Pan *et al.* also developed a penguin-inspired robot with independent control of left and right feathering, achieving quick turns at 73°/s [17]. However, its flapping amplitude was smaller compared to real penguins, and a slower swimming speed of 0.5 m/s.

In our previous study, we developed a penguin-mimetic wing mechanism capable of independently controlling feathering and flapping with large amplitudes based on detailed motion analysis of real penguins [18, 19]. Both the magnitude and direction of the hydrodynamic force of the wing can be largely changed by feathering and tilting the flapping axis [18]. However, the mechanism relied on commercial, nonwaterproof servomotors, which hindered successful underwater operation. Traditional sealing using an O-ring at the motor output shaft are undesirable due to the high friction needed for deep dives under high water pressure. Additionally, the periodic changes in the motor's rotational direction required for flapping are not well-suited to O-ring sealing.

A promising method for ensuring water resistance is the use of submersible brushless motors. Some underwater drones use these motors to directly rotate propellers at high frequencies [20–23]. However, penguin-mimetic wing motions require low frequency, high-torque, and precise control, which differ significantly from the demands of the rotating propellers. Therefore, the development of submersible geared servomotors that meet these specific requirements is highly desirable.

In this work, we developed in-house submersible geared servomotors based on our previous research [24] and implemented them in our 2-DoF penguin-mimetic wing mechanism capable of controlling both flapping and feathering [18]. The motors requirements were determined through quasi-steady hydrodynamic calculations. A prototype of a robotic penguin, built to the same size as a gentoo penguin [19], was equipped with the submersible wing mechanism was on each side of the wing. We tested the swimming performance of the robot in a swimming pool and the results demonstrated that various agile maneuvers, such as rapid acceleration, hard braking, rolling, pitching, and yawing, were realized solely by adjusting the feathering motions. This prototype will serve as a testbed for further studies on maneuverability using more

This work was supported by JSPS KAKENHI Grant-in-Aid for Scientific Research on Innovative Areas "Science of Soft Robots" project under Grant Number JP18H05468 and JKA through its promotion funds from KEIRIN RACE.

Taiki Shimooka and Hiroto Tanaka are with Institute of Science Tokyo, Tokyo, Japan. Atsushi Kakogawa is with Ritsumeikan University, Shiga, Japan.

Hiroto Tanaka is a corresponding author to provide e-mail: tanaka.h.cb@m.titech.ac.jp.

complex wing motions that combine both feathering and flapping.

II. Mechanical Design of the Robotic Penguin

A. Overview

The designs of the robotic penguin and the wing mechanism are shown in Fig. 1. The body has a symmetric spindle shape with a length of 0.72 m and a diameter of 0.24 m. Flapping and feathering motions are generated by the difference in rotational speed between two geared servomotors using differential gears. The mechanical principle is the same as in our previous work [18], though the third motor, which was previously used for pitching the flapping axis, was omitted in this study to simplify the design, fabrication, and experimentation for the prototype.

The flapping angle, θ_{flap}, and feathering angle, θ_{feather}, are expressed as $\theta_{\text{flap}} = (\theta_2 - \theta_1)/2$ and $\theta_{\text{feather}} = (\theta_1 + \theta_2)/2$, respectively, where θ_1 and θ_2 are the rotational angles of each motor (Fig. 1(b)).

The *XYZ* body coordinate was defined with the *X*-axis as the longitudinal axis of the body, the *Y*-axis as the lateral axis, and the *Z*-axis as the dorsoventral axis. This origin matches the geometric center of the spindle body, excluding the stabilizing tail. The flap-feather coordinate system $X_F Y_F Z_F$ was created by shifting the *XYZ* coordinates to the intersection of the flapping and feathering rotation axes. The X_F-axis aligns with the flapping rotation axis, and the Y_F-axis coincides with the feathering rotation axis when $\theta_{\text{flap}} = 0°$. The $X_W Y_W Z_W$ coordinate system was defined by rotating the $X_F Y_F Z_F$ coordinate system around the X_F-axis by θ_{flap} and around the Y_F-axis by θ_{feather}, such that the $X_W Y_W$ plane matches the wing plane (Fig. 2 (a)). The θ_{flap} of each wing can range from −180° to 180°, where $\theta_{\text{flap}} = 0°$ indicates that the wing points laterally (Fig. 1(b)). This amplitude is larger than that previously reported for a penguin carcass, where the maximum θ_{flap} was 45° [25]. Moreover, our θ_{feather} is unrestricted, which exceeds the movement range of real penguin.

B. Hydrodynamics Calculation

The hydrodynamic forces acting on the wing and body were calculated to determine the required torque and speed for the geared motors. Assuming that the robotic penguin moves forward along the *X*-axis, with symmetric motions of the left and right wing, and that its weight balances the buoyancy, the equation of translational motion can be expressed as:

$$Ma = 2F_{\text{wing},\,x} - F_{\text{body, drag}} \qquad (1),$$

where *M* is the mass, *a* is acceleration, $F_{\text{wing},\,x}$ is the forward component of the hydrodynamic force of each wing and $F_{\text{body, drag}}$ is the body's drag.

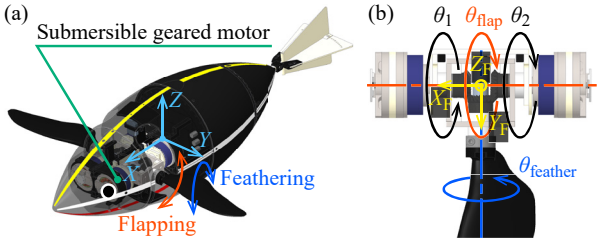

Fig. 1 (a) Overview of our robotic penguin. (b) Penguin-mimetic 2-DoF wing mechanism.

The hydrodynamic force acting on the wing, F_{wing} was obtained by quasi-steady calculations as a sum of the lift, drag, and added mass force vectors, following the calculation method used for real penguins [25]. The wing model was created using 3-D scan data of a gentoo penguin wing, modified by eliminating the camber and torsion to form a symmetric airfoil. The wing was divided into 10 elements of equal width (Fig. 2). The chord length, width, and area of each element as c_j [m], r_j [m], and S_j [m^2], respectively, where j is the element number. The wing length $\Sigma\, r_j$ was 252 mm, and the wing area $\Sigma\, S_j$ was 0.0136 m^2.

The lift $F_{\text{wing, lift}}$ [N] and drag $F_{\text{wing, drag}}$ [N] of the wing were calculated as

$$F_{\text{wing, lift}} = \frac{1}{2}\rho \sum_{j=1}^{10} C_{\text{L},\,j}\alpha_j S_j \left\|\boldsymbol{v}_{\text{in},\,j}\right\|^2 \qquad (2),$$

$$F_{\text{wing, drag}} = \frac{1}{2}\rho \sum_{j=1}^{10} C_{\text{D},\,j}\alpha_j S_j \left\|\boldsymbol{v}_{\text{in},\,j}\right\|^2 \qquad (3),$$

where $\boldsymbol{v}_{\text{in},\,j}$ [m/s] is the relative flow velocity of the element, and α_j [°] is the AoA for each element (Fig. 3 (a), (b)). The value of $\boldsymbol{v}_{\text{in},\,j}$ was obtained as reverse vector of the moving velocity of the element, assuming that the surrounding water is stationary. The angle α_j is the angle between $\boldsymbol{v}_{\text{in},\,j}$ and the wing plane. The lift $C_{\text{L},\,j}$ and drag $C_{\text{D},\,j}$ coefficients for each element were expressed as

$$C_{\text{L},\,j} = 2.80 \sin \alpha_j \cos \alpha_j \qquad (4),$$

$$C_{\text{D},\,j} = 2.80 \sin^2 \alpha_j \qquad (5),$$

as shown in Fig. 2 (c). These coefficients were determined based on steady wing characteristics and the cross-flow vortex model, which assumes that the flow does not separate from the wing even at large AoA values [19, 26]. The added mass force $F_{\text{wing, am}}$ [N] was calculated by:

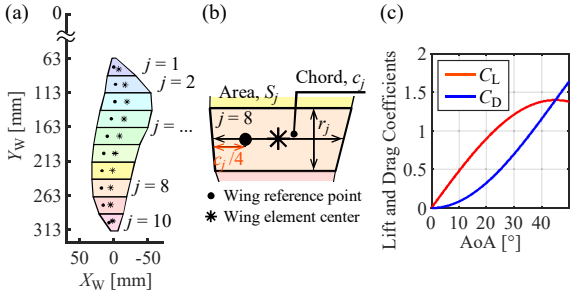

Fig. 2 (a) Planar outline of the wing and wing elements for hydrodynamics calculation. (b) Dimension parameters in each wing element. (c) The lift and drag coefficients.

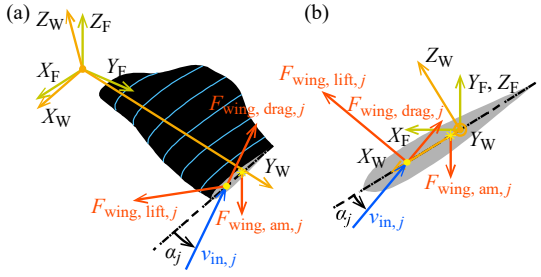

Fig. 3 Schematics of the hydrodynamic forces and the AoA. (a) Orthogonal view. (b) Cross-sectional view of the example element.

$$F_{\text{wing, am}} = \frac{1}{4}\rho\pi \sum_{j=1}^{10} c_j^2 r_j a_{\text{WC, }j} \qquad (6),$$

where $a_{\text{WC, }j}$ [m/s^2] is the acceleration component of the element normal to the wing plane. The spatial relationships among these parameters are visually summarized in Fig. 3 (a) and (b). Details of the above quasisteady calculation method are explained in our previous paper on real penguins [19].

The body's drag, $F_{\text{body, drag}}$ is calculated via the following equations:

$$F_{\text{body, drag}} = \frac{1}{2}\rho C_{\text{D, body}} S_{\text{body, front}} U^2 \qquad (7),$$

where $S_{\text{body, front}}$ and U denote the frontal projected area and the forward velocity of the body, respectively. The drag coefficient of the body, $C_{\text{D, body}} = 0.255$, was obtained from drag measurements using a 25% small-scale model in a water tunnel at a Reynolds number of 5.0×10^5 for the body length. The Reynolds number of the robot during maximum speed swimming was 1.5×10^6, as described in Section III. B. According to previous studies on drag measurements with similar bodies [27], the difference in C_D between actual and small-scale bodies is assumed to be small within this range of Reynolds numbers.

The translational motion of the robot was simulated using Equation (1) $F_{\text{wing, }x}$ and $F_{\text{body, drag}}$ which were determined at each time step with an internally developed MATLAB (MathWorks, the United States) script. The time interval was set to 0.01 s. The following function was defined as the wing motion that requiring the most motor power: $\theta_{\text{flap}} = A_{\text{flap}} \sin(2\pi ft - \pi/2)$ and $\theta_{\text{feather}} = A_{\text{feather}} \sin(2\pi ft)$, where A_{flap}, A_{feather}, and frequency f were 60°, 30°, and 2.0 Hz, respectively. A_{flap} and A_{feather} were larger than those observed in real penguins ($A_{\text{flap}} = 37°$, $A_{\text{flap}} = 16°$ on average [19]), while f was similar (2.0 Hz on average [19]).

As a result, the robot rapidly accelerated to 1.68 m/s within just two flapping cycles over 1.0 s (Fig. 4(a)). The final speed after the fourth cycle was calculated to be 1.75 m/s. The required maximum torque and rotation speed of the motor were approximately 8 Nm and 140 rpm, respectively (Fig. 4(b)).

C. Design and Fabrication of the Submersible Geared Servomotor and Robotic penguin

The fabricated submersible geared servomotor is shown in Fig. 5. It consists of a brushless DC motor (RI50 KV100, CubeMars Co., Ltd., China) and an in-house two-stage planetary gear reducer with a reduction ratio of 13.44, designed to meet the torque and speed requirements. The Hall sensors and magnetic encoders were encapsulated in epoxy resin (Fig. 5 (c) and (d)). The total mass was 243 g, including 105 g for the reducer.

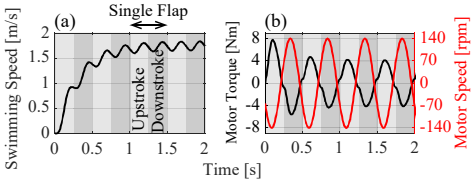

Fig. 4 Results of the numerical simulation. (a) Swimming speed. (b) The torque and speed required for each motor.

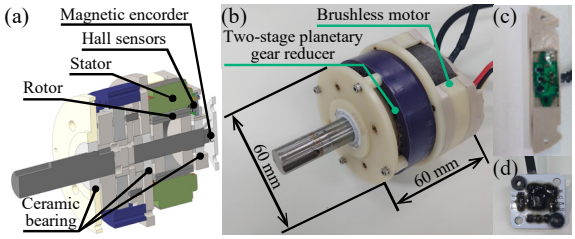

Fig. 5 (a) Internal structure of our submersible geared servomotor. (b) Photo of the fabricated servomotor. The hall sensors (c) and magnetic encoder (d) were embedded in epoxy resin for waterproof.

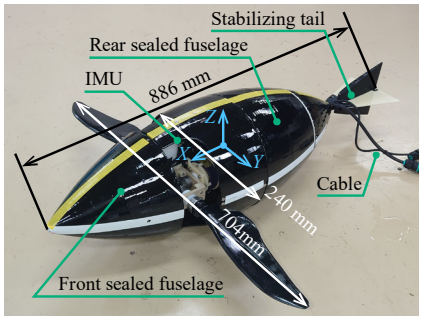

Fig. 6 The completed robotic penguin.

An overview of the completed robotic penguin is shown in Fig. 6. The front-sealed fuselage was left empty to provide buoyancy and adjust the center of gravity. The rear-sealed fuselage contained the motor drivers (ESCON 70/10, Maxon Co., Ltd., Switzerland) and a microcontroller (Nucleo F767ZI, STMicroelectronics N.V., Switzerland). Additional metal weights totaling 2.28 kg were placed in the middle open fuselage to adjust the buoyancy, ensuring it exceeded the total weight of the robot by 22.5 N. All cables from the motors in the middle fuselage were connected to the motor drivers through cable glands, ensuring water-tight connections. The LAN and power cables extend from the rear of the fuselage for communication with an external computer and power supply. The communication protocol between the microcontroller and PC used the Transmission Control Protocol (TCP) at 83.3 Hz. Power was supplied to the motor drivers by a 48 V switching power supply (AEA1000F-48, COSEL Co., Ltd., Japan). The rotational angles of each motor were controlled using a Proportional-Derivative (PD) feedback controller. To minimize the effect of external cable tension on the robot's swimming maneuvers, several floats were attached to the cables at intervals to achieve neutral buoyancy. However, it was still observed that the cables slightly pulled the robot and affected yaw and pitch rotations. This issue should be resolved in future work.

The resultant XYZ coordinates of the gravity center of the body were $x_g = -11.1$ mm, $y_g = 1.15$ mm, and $z_g = -1.07$ mm, which closely matched the geometric center of the body. Additionally, vertical and horizontal tail wings were attached to the end of the body. The robot's total mass was 9.53 kg, including 2.28 kg of weight. This mass falls between that of king penguins (11.9 kg [13]) and gentoo penguins (5.5 kg [13]).

III. Swimming Experiment

A. Experimental Setup

The experiment was conducted in an indoor swimming pool at the Institute of Science Tokyo. The water depth and

temperature were approximately 2 m and 28.3 °C, respectively. Five waterproof video cameras (GoPro Hero9, GoPro Inc., USA) were placed in parallel along the sidewall at a depth of 0.4 m with intervals of either 0.5 m or 1 m. These cameras were labeled Cameras 1 through 5 (Fig. 7). The robot started in front of Camera 1 and the swimming speed was measured as the robot passed through the line of sight of each camera. θ_{flap} and $\theta_{feather}$ during swimming were measured using magnetic encoders attached to the motors, while the current flowing to each motor was measured by a motor driver. The angular velocity of the robot was recorded by a waterproof wireless motion logger (WAVE TRACK, COMETA, Italy) attached to the middle fuselage (Fig. 6). The posture angle was calculated by integrating the measured angular velocity.

B. Forward Propulsion

The wing motions were set as $\theta_{flap} = 60° \sin(2\pi ft - \pi/2)$, $\theta_{feather} = A_{feather} \sin(2\pi ft)$, and $f = 2.0$ Hz. $A_{feather}$ was changed from 10° to 60° with 10° increments. Fig. 8 shows an example of the target and measured angles for $A_{feather} = 30°$. The measured θ_{flap} and $\theta_{feather}$ lagged behind the target angles by only 0.005 s (1% of $1/f$), and the measured amplitudes of θ_{flap} and $\theta_{feather}$ were smaller than the target amplitudes by just 2° (3.3% of 60°) and 1.7° (5% of 30°), respectively.

The measured speeds are summarized in Fig. 9(a). The initial speed immediately after the start of swimming during one and a half flapping cycles was highest with an $A_{feather}$ of 50° (0.7 m/s). However, as the robot swam forward, a smaller $A_{feather}$ led to higher swimming speeds. The maximum speed was 1.8 m/s with an $A_{feather}$ of 20° in the fourth and fifth flapping cycles. Fig. 9 (b) shows the calculated AoA at wing element of $j = 8$ at the middle of the upstroke for each swimming speed. When the AoA was within a range from 26° to 47°, swimming speed was relatively high. This AoA range would provide a relatively large lift with not too large drag (Fig. 2 (c)). For reference, previous tethered experiments with a 40%-sized wing reported that the thrust was maximized with an AoA of approximately 20° [18]. This difference between these findings and the current results might be due to the vertical motion of the body. In the present calculation of the AoA, the speed of the body perpendicular to the swimming

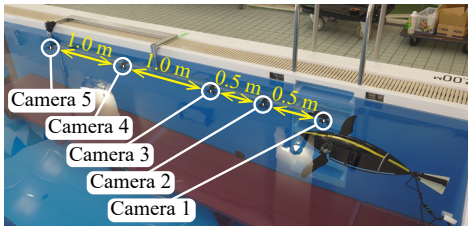

Fig. 7 Positions of the five cameras for speed measurement.

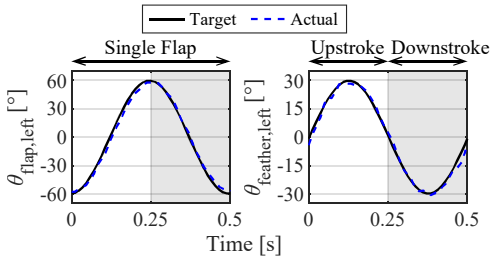

Fig. 8 The target and measured angles of the flapping angle (a) and the feathering angle (b) during forward swimming.

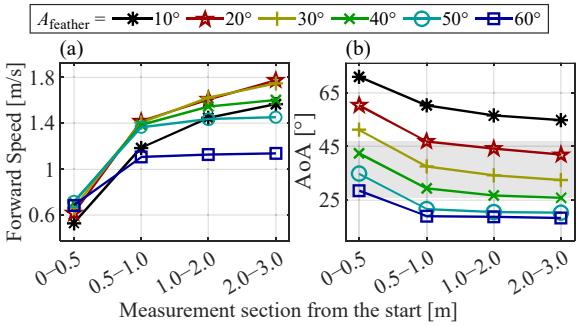

Fig. 9 The swimming speed (a) and angle of attack (b) for each feathering amplitude and at each interval. The black circle represents the fastest point at each interval.

Table 1 The CoT for each feathering amplitude at its maximum speed.

$A_{feather}$ [°]	10	20	30	40	50	60
CoT [J/kg·m]	47.8	36.2	26.6	21.8	16.9	15.1

direction was not considered, leading to an overestimation of the AoA. In addition, the Reynolds numbers differed: the Reynolds number based on the mean chord at the maximum speed of 1.8 m/s was 2.2×10^5, whereas that of the previous tethered experiments was 3.2×10^4.

The cost of transport (CoT) [J/kg·m] was calculated for travel from cameras 3 to 4, dividing the consumed power by the travel distance and total mass. The CoT is a metric used to evaluate the propulsion efficiency of animals and transport machines [2, 3, 28] (Table 1). A large $A_{feather}$ led to a lower CoT, indicating better efficiency. This finding demonstrates the trade-off between maximum speed and efficiency, which can be managed through active feathering control. Additionally, the implementation of flexible wings would improve the efficiency [19].

The CoT of our robotic penguin (15.1–47.8 J/kg·m) is comparable to that of previous robotic fish, whose CoT ranged from 12.7 to 35 J/kg·m [2, 3].

C. Rolling, Pitching, Yawing, and Stopping Maneuvers

To demonstrate the agility of the robotic penguin through independent control of wing feathering, roll, pitch, and yaw rotations were performed. In each turn, the wings were operated for 1 second. θ_{flap} and f were constant at $\theta_{flap} = 60° \sin(2\pi ft - \pi/2)$ and 2 Hz, respectively. Fig. 10 shows the schematics of the rolling, pitching, yawing, and braking mechanisms illustrating wing motions and the directions. of the forces generated during these maneuvers.

Quick rolling was realized, as shown in Fig. 11. The target $\theta_{feather}$ was set as $\theta_{feather} = 90°$ (during the upstroke) or 0° (during the downstroke). The maximum roll angular velocity was 682°/s, and the average velocity during the second flapping cycle was 363°/s. This velocity is much faster than the average roll angular velocity of previous robotic fish designed for agile swimming (80°/s) [4].

Downward pitching was also achieved by changing only feathering with constant flapping (Fig. 12). The target $\theta_{feather}$ was set as ($\theta_{feather} = 440° \; t - 55°$) during the upstroke and ($-440° \; t + 55°$) during the downstroke, where t denotes the time from the beginning of each feathering cycle. The maximum pitch angular velocity and the average of the second flapping cycle were 152°/s and 75°/s, respectively. The

maximum rate was approximately half that of an agile dolphin robot (304°/s) [6]. Notably, this feathering pattern is unlikely in real penguins. In penguins, θ_{feather} is positive during the upstroke and negative during the downstroke to generate forward thrust, as shown in Fig. 8 (b). However, in the first half of the upstroke during the present pitch, θ_{feather} was negative enough to generate a backward force (Fig. 10 (b)). Moreover, θ_{feather} during the downstroke went below −90°, which is impossible for real penguins. This suggests that wing feathering can potentially achieve agility beyond that of real penguins.

Quick counterclockwise yawing was also realized by generating the backward thrust of the left wing with unconventional feathering pattern (Fig. 13). The target θ_{feather} was set as $\theta_{\text{feather}} = -60° \sin(2\pi ft) + 180°$, and $f = 2.0$ Hz. The maximum yaw angular velocity and the average during the second flapping cycle were 150°/s and 92°/s, respectively, comparable to the performance of an agile robotic manta (max. 140°/s, avg. 109°/s) [7].

Both rolling and forward propulsion were simultaneously realized by modifying θ_{feather} for simple rolling so that the mean of θ_{feather} was 30° for the left wing and −30° for the right wing (Fig. 14). The speed between Cameras 1 and 2 was 0.7 m/s, and the rolling rate during the third and fourth flapping cycles was 401°/s.

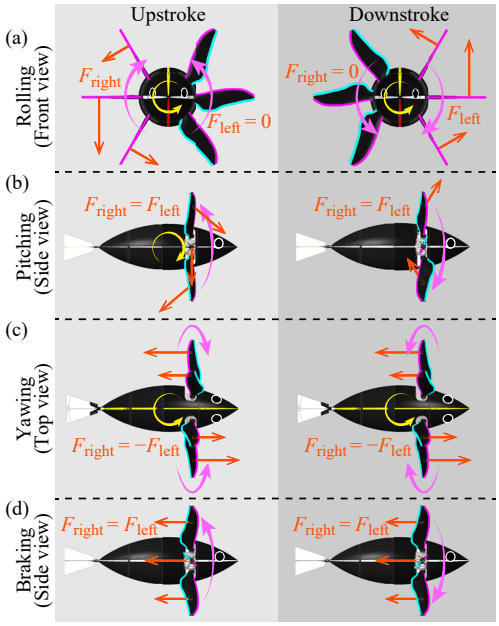

Fig. 10 Postures and force directions of the wings for rolling (a), pitching (b), yawing (c), and braking (d). The red arrow indicates the direction of force, the yellow arrow shows the direction of body rotation, and the magenta arrow represents the direction of wing flapping. The leading edge of the wing is indicated in magenta and the trailing edge in cyan.

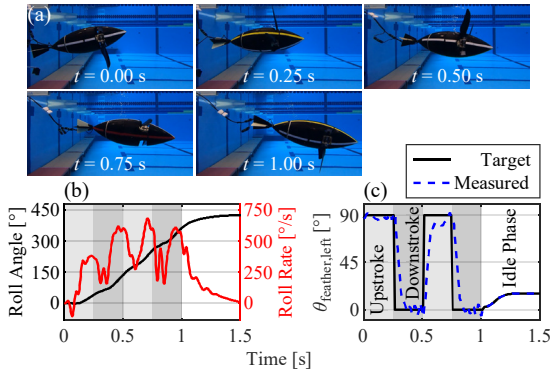

Fig. 11 (a) Snapshots of clockwise rolling. (b) Roll posture angle and roll angular velocity, (c) feathering angle during clockwise rolling.

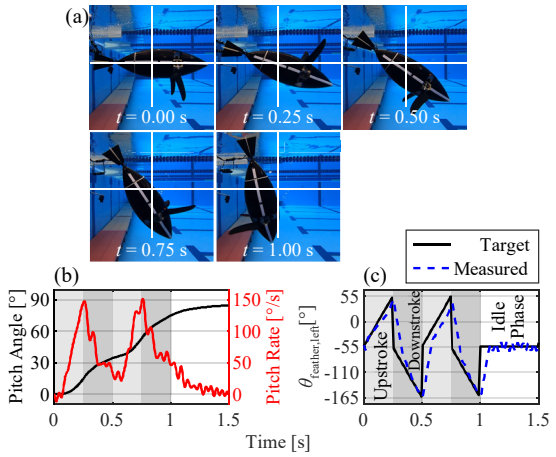

Fig. 12 (a) Snapshots of downward pitching. (b) Pitch posture angle and pitch angular velocity, (c) feathering angle during downward pitching.

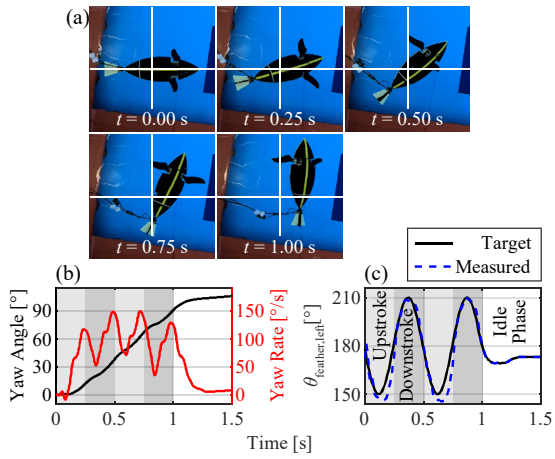

Fig. 13 (a) Snapshots of counterclockwise yawing. (a) Yaw posture angle and yaw angular velocity, (b) feathering angle during counterclockwise yawing.

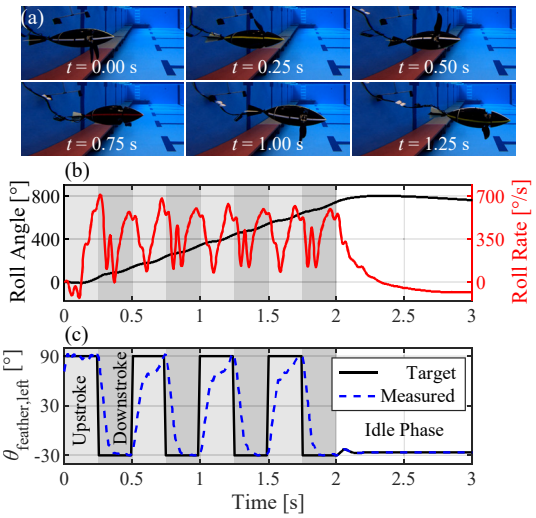

Fig. 14 (a) Snapshots of rolling forward swim. (b) Roll posture angle and roll angular velocity, (c) feathering angle during rolling forward swim.

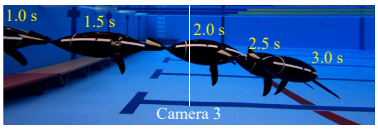

Fig. 15 Overlaid snapshots of hard braking. Time is counted from the start.

Finally, hard braking through the backward thrust of both wings was demonstrated, as shown in Fig. 15. After forward swimming with a feathering angle of 30° for four flapping cycles, θ_{feather} was set as $\theta_{\text{feather}} = 30° \sin(2\pi ft + \pi)$, followed by another two additional flapping cycles, reducing the speed to almost zero. Assuming an entry speed before braking was 1.75 m/s (Fig. 9(a)) and a terminal speed of less than 0.1 m/s, the deceleration rate was calculated to be 1.7 m/s^2. This hard braking by backward thrust is not achievable by real penguins.

IV. Conclusion

A full-scale robotic penguin driven by submersible geared servomotors was developed based on hydrodynamic calculations. The robot had a pair of 2-DoF wings, enabling independent control of wing flapping and feathering. Underwater swimming tests demonstrated that independent feathering control enabled high-speed propulsion and agile maneuvers. The robot could accelerate to a maximum speed of 1.8 m/s (equivalent to 2.0 body length per second) in just four flapping cycles. It also achieved quick rolling, pitching, and yawing in place with average angular velocities of 363°/s for rolling, 75°/s for pitching, and 92°/s for yawing. Additionally, unique rolling propulsion at 0.7 m/s speed and 401°/s rolling rate was demonstrated. Furthermore, hard braking from 1.8 m/s to complete stop within 1 second was achieved using backward thrust, a maneuver that is impossible for real penguins.

Further agility and efficiency are expected to be realized by introducing flapping control in addition to the present feathering control. Our robot showcases the potential of wing-propelled penguin-inspired underwater robots and will serve as a testbed for both robotics and biological studies.

Acknowledgment

The authors thank Kaya-Tech-Studio for their contribution in developing the software for the robotic penguin.

References

[1] F. E. Fish, "Advantages of Aquatic Animals as Models for Bio-inspired Drones over Present AUV Technology," *Bioinspiration & Biomimetics*, vol. 15, no. 2, 2020.

[2] J. Zhu, C. White, D. K. Wainwraight, V. Di. Santo, G. V. Lauder and H. Bart-Smith, "Tuna Robotics: A High-frequency Experimental Platform Exploring the Performance Space of Swimming Fishes," *Science Robotics*, vol. 4, Issue. 34, 2019.

[3] T. J. K. Ng, N. Chen and F. Zhang, "Snapp: An Agile Robotic Fish with 3-D Maneuverability for Open Water Swim," *IEEE Robotics and Automation Letters*, vol. 8, no. 10, pp. 6499–6506, 2023.

[4] S. Zhang, Y. Qian, P. Liao, F. Qin and J. Yang, "Design and Control of an Agile Robotic Fish with Integrative Biomimetic Mechanisms," *IEEE/ASME Transactions on Mechatronics*, vol. 21, no. 4, pp. 1846–1857, 2016.

[5] Y. Zhong, Z. Li and R. Du, "A Novel Robot Fish with Wire-Driven Active Body and Compliant Tail," *IEEE/ASME Transactions on Mechatronics*, vol. 22, no. 4, pp. 1633–1643, 2017.

[6] J. Yu, Z. Su, M. Wang, M. Tan and J. Zhang, "Control of Yaw and Pitch Maneuvers of a Multilink Dolphin Robot," *IEEE Transactions on Robotics*, vol. 28, no. 2, pp. 318–329, 2012.

[7] Y. Meng, Z. Wu, D. Chen, P. Zhang, M. Tan and J. Yu, "Development and 3-D Path-Following Control of an Agile Robotic Manta with Flexible Pectoral Fins," *IEEE Transactions on Cybernetics*, 2023.

[8] Y. Wang, P. Zhang, H. Huang and J. Zhu, "Bio-Inspired Transparent Soft Jellyfish Robot," *Soft Robotics*, vol. 10, no. 3, pp. 590–600, 2023.

[9] M. A. Robertson, F. Efremov and J. Paik, "RoboScallop: A Bivalve Inspired Swimming Robot," *IEEE Robotics and Automation Letters*, vol. 4, no. 2, pp. 2078–2085, 2019.

[10] A. Azuma, "The Biokinetics of Flying and Swimming Second Edition," *Second ed*. (*AIAA Education Series*). Virginia: AIAA, 2006.

[11] N. Kato, "Median and Paired Fin Controllers for Biomimetic Marine Vehicles," *Applied Mechanics Reviews*, vol. 58, Issue. 4, pp. 238–252, 2005.

[12] M. Sfakiotakis, D. M. Lane and J. B. C. Davies, "Review of Fish Swimming Modes for Aquatic Locomotion," *IEEE Journal of Oceanic Engineering*, vol. 24, no. 2, pp. 237–252, 1999.

[13] K. Sato, Watanuki. Y, Takahashi. A, Miller. P. J. O, Tanaka. H, Kawabe. R, Ponganis. P. J, Handrich. Y, Akamatsu. T, Watanabe. Y, "Stroke Frequency, but not Swimming Speed, is Related to Body Size in Free-ranging Seabirds, Pinnipeds and Cetaceans," *Proceedings of the Royal Society B*, vol. 274, Issue. 1609, pp. 471–477, 2006.

[14] T. Mattern, K. Pütz, P. Garcia-Borboroglu, U. Ellenberg, D. M. Houston, R. Long, B. Lüthi and P. J. Seddon, "Marathon Penguins – Reasons and Consequences of Long-range Dispersal in Fiordland Penguins / Tawaki during the Pre-moult Period," *PLOS ONE*, vol. 13, no. 8, 2018.

[15] C. A. Hui. "Maneuverability of the Humboldt Penguin (*Spheniscus Humboldti*) during Swimming," *Canadian Journal of Zoology*, 63(9): 2165–2167, 1985.

[16] W. Stoll, "Aquapenguin," FESTO, Esslingen, Germany, Tech. Rep. 54711/EN, 2009.

[17] J. Pan, Z. Zhou, J. Wang, P. Zhang and J. Yu, "Development of a Penguin-Inspired Swimming Robot with Air Lubrication System," *IEEE Transactions on Industrial Electronics*, vol. 70, no. 3, pp. 2780–2789, 2023.

[18] Y. Shen, N. Harada, S. Katagiri and H. Tanaka, "Biomimetic Realization of a Robotic Penguin Wing: Design and Thrust Characteristics," *IEEE/ASME Transactions on Mechatronics*, vol.26, pp.2350–2361, 2021.

[19] N. Harada, T. Oura, M. Maeda, Y. Shen, D. M. Kikuchi and H. Tanaka, "Kinematics and Hydrodynamics Analyses of Swimming Penguins: Wing Bending Improves Propulsion Performance," *Journal of Experimental Biology*, vol. 224, 2021.

[20] R. Bogue, "Underwater Robots: a Review of Technologies and Applications," *Industrial Robot*, vol. 42, Issue. 3, pp. 186–191, 2015.

[21] C. Kai, Z. Weiwei and D. Lu, "Research on Mobile Water Quality Monitoring System Based on Underwater Bionic Robot Fish Platform," 2020 *IEEE International Conference on Advances in Electrical Engineering and Computer Applications* (*AEECA*), pp. 457–461, 2020.

[22] B. Hur, D. Malawey, J. A. Morgan and C. Ma, "3-D Printed Metal and Plastic Propeller Design and Manufacturing for Smallscale Underwater Thrusters," *ASEE Annual Conference & Exposition*, Paper ID #26855, 2019.

[23] J. Neira, C. Sequeiros, R. Huamani, E. Machaca, P. Fonseca and W. Nina, "Review on Unmanned Underwater Robotics, Structure Designs, Materials, Sensors, Actuators, and Navigation Control," *Journal of Robotics*, vol. 2021, Article ID 5542920, 2021.

[24] S. D. Rajendrakumar, A. Kakogawa and S. Ma, "An Underwater Snake Robot that Does Not Consider Actuators' Waterproof: Design and Primary Experiments," 2023 *IEEE International Conference on Robotics and Biomimetics* (*ROBIO*), Koh Samui, Thailand, 2023.

[25] R. Bannasch, "Hydrodynamics of Penguins – an Experimental Approach," *The Penguins: Ecology and Management*, pp. 141–176, 1995.

[26] P. R. Bandyopadhyay, D. N. Beal and A. Menozzi, "Biorobotic Insights into How Animals Swim," Journal of Experimental Biology, vol. 211, no. 2, pp. 206–214, 2008.

[27] S. F. Hoerner, "Fluid-Dynamic Drag," 1965.

[28] K. Schmidt-Nielsen, "Locomotion: Energy Cost of Swimming, Flying, and Running," *Science*, vol. 177, no. 4045, pp. 222–228, 1972.